Influence of Divalent Cations in the Protein Crystallization Process Assisted by Lanthanide-Based Additives

Amandine Roux, Romain Talon, Zaynab Alsalman, Sylvain Engilberge, Anthony D'Aléo,
Sebastiano Di Pietro, Adeline Robin, Alessio Bartocci, Guillaume Pilet, Elise Dumont, Tristan Wagner,
Seigo Shima, François Riobé,* Eric Girard,* and Olivier Maury*

ACCESS | 📊 Metrics & More | 📰 Article Recommendations | 🔵 Supporting Information

ABSTRACT: The use of lanthanide complexes as powerful auxiliaries for biocrystallography prompted us to systematically analyze the influence of the commercial crystallization kit composition on the efficiency of two lanthanide additives: $[Eu(DPA)_3]^{3-}$ and Tb-Xo4. This study reveals that the tris(dipicolinate) complex presents a lower chemical stability and a strong tendency toward false positives, which are detrimental for its use in a high-throughput robotized crystallization platform. In particular, the crystal structures of $(Mg(H_2O)_6)_3[Eu(DPA)_3]_2 \cdot 7H_2O$ (**1**), $\{(Ca(H_2O)_4)_3[Eu(DPA)_3]_2\}_n \cdot 10nH_2O$ (**2**), and $\{Cu(DPA)(H_2O)_2\}_n$ (**3**), resulting from spontaneous crystallization in the presence of a divalent alkaline-earth cation and transmetalation, are reported. On the other hand, Tb-Xo4 is perfectly soluble in the crystallization media, stable in the presence of alkaline-earth dications, and slowly decomposes (within days) by transmetalation

with transition metals. The original structure of $[Tb_4L_4(H_2O)_4]Cl_4 \cdot 15H_2O$ (**4**) is also described, where L represents a bis(pinacolato)triazacyclononane ligand. This paper also highlights a potential synergy of interactions between Tb-Xo4 and components of the crystallization mixtures, leading to the formation of complex adducts like {AdkA/Tb-Xo4/Mg^{2+}/glycerol} in the protein binding sites. The observation of such multicomponent adducts illustrated the complexity and versatility of the supramolecular chemistry occurring at the surface of the proteins.
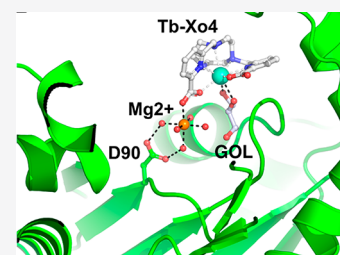
INTRODUCTION

During this past decade, the number of protein crystal structures deposited in the Protein Data Bank (PDB; https://www.rcsb.org/) has increased steadily despite the emergence of alternative techniques, like NMR or cryo-electron microscopy, and almost 90% of new deposited structures are elucidated using X-ray crystallography. However, this last method still suffers from two major chokepoints that severely reduce the efficiency of its implementation: (i) the production of high-quality single crystals and (ii) the phase determination mandatory for electron density map calculation.[1−3] Currently, the structural genomics statistics estimated that only 10% of the purified proteins will see their structure elucidated; consequently, there is considerable room for improvement.[2] To tackle these drawbacks, most developments are concentrated in the field of technology with improvement of the structure determination pipelines, more intense radiation sources or the use of an X-ray free-electron laser source to address even smaller crystals, and the routine use of high-throughput crystallization platforms to screen an even larger number of conditions with a reduced amount of sample.[4,5] Unfortunately, a certain success of these developments led, in comparison, to neglect of traditional methodological approaches. In particular, the research for new additives that can solve either the crystallization or the phase determination problems or better both simultaneously is a

real promising route for improvement in the field for a moderate cost.

Indeed, it is well-known that the incorporation in a protein crystal of a well-ordered heavy atom enables one to solve the phase problem using anomalous-based methods: single-wavelength anomalous dispersion (SAD) and multiwavelength anomalous dispersion (MAD).[6] These heavy atoms can be implemented in a covalent way, as pioneered by Doublié's S-to-Se replacement using selenomethionine, or in a noncovalent way using transition-metal salts (Hg, Pt, etc.) or lanthanide complexes.[7] On the other hand, the development of additives to facilitate the nucleation process was initially focused on heterogeneous compounds like minerals, natural materials such as horse and human hair, nanoporous materials,[8,9] and, more recently, molecular imprinted polymers.[10,11] However, these heterogeneous nucleants are insoluble and therefore are hardly compatible with the generalized homogeneous high-throughput crystallization methods used nowadays.
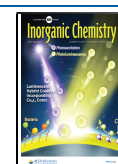
Recently, new soluble additives were developed that are fully compatible with the above-mentioned robotized crystallization screening systems (Figure 1): (i) the polyoxometalates
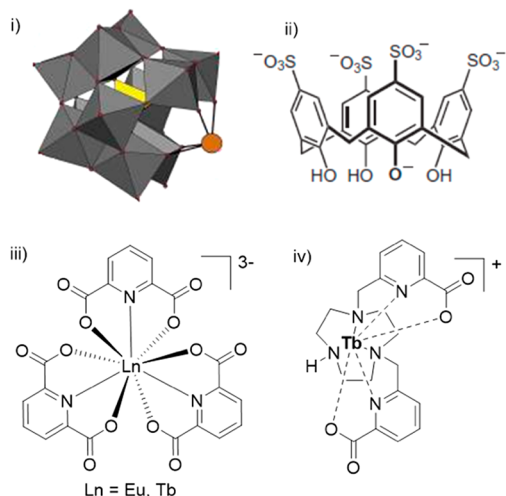

Figure 1. Select examples of the three families of soluble additives used in protein crystallography: (i) Keggin polyoxometalate structure of $[Ce(\alpha\text{-}PW_{11}O_{39})_2]^{10-}$; (ii) p-sulfonatocalix[4]arene (slx4) and lanthanide derivatives studied in this work; (iii) tris(dipicolinate) $[Ln(DPA)_3]^{3-}$; (iv) crystallophore Tb-Xo4.

developed by Rompel and co-workers,[12-15] (ii) the anionic macrocycles proposed by the team of Crowley (phosphonated or sulfonatocalix[n]arenes (n = 4, 6, 8), cucurbituril, etc.),[16-19] and the lanthanide complexes (iii) tris(dipicolinate) ([Ln-(DPA)_3]^{3-})[20] and (iv) crystallophore (Tb-Xo4),[21] reported by our group. All of these species can be considered to be "molecular glues", inducing a network of supramolecular interactions with proteins in solution and favoring crystalline contacts in the crystal packing. Among these three families of additives, polyoxometalate and lanthanide complexes contain heavy atoms (tungsten, europium, or terbium, respectively) and can therefore simultaneously solve the nucleating and phase determination issues using conventional SAD/MAD methods, whereas phase determination based on S-SAD using sulfocalix[n]arene has been recently reported.[22] In particular, on the basis of our own statistics obtained on 20 soluble proteins, the crystallophore increases the number of crystallization conditions by a factor of 3–7,[21] gives better-quality crystals by generally suppressing the twinning issue, and enables de novo phasing in more than 80% of the cases, even in complicated ones where selenation was unsuccessful.[23] Furthermore, Tb-Xo4 was also shown to be compatible with microseeding, counterdiffusion crystallization methods, and serial crystallography (the mesh-and-collect method).[23,24] Both $Na_3[Eu(DPA)_3]$ and Tb-Xo4 are now available and frequently exploited by the biocrystallography community to solve the structure of the protein of biological interest either for nucleation and/or for phasing steps.[25-31] As a consequence, they have been involved in crystallization processes according to the state-of-the-art high-throughput protocols using pipetting robots and conventional commercial kits. During the course of these studies, several results have been obtained, suggesting interaction of the lanthanide complexes with the crystallization condition mixtures, which can lead to false-positive or apparent cooperative behaviors favoring the lanthanide complex/protein interaction.

In this paper, we describe two representative examples of such behavior: a false positive observed during crystallization of the Acriflavine-resistant protein B from *Escherichia coli* (Ec-AcrB) in the presence of $Na_3[Eu(DPA)_3]$ and an apparent cooperative behavior in the crystal structure of adenylate kinase protein from *Methanothermococcus thermolithotrophicus* (AdKA) in the presence of Tb-Xo4. In order to rationalize these results, we explored the behavior of our lanthanide-based additives in conventional crystallization kits in the absence of protein, with a particular focus on the role of divalent alkaline-earth or transition-metal dications, and evidenced detrimental autocrystallization processes and transmetalation reactions.

■ RESULTS AND DISCUSSION

The crystallization of Ec-AcrB, a homotrimeric membrane protein (341 kDa) whose structure was already described (PDB 2GIF), was performed in the presence and absence of $Na_3[Eu(DPA)_3]$ using a high-throughput crystallization facility (HTXlab, EMBL, Grenoble, France) with six commercial crystallization kits (see the experimental details). The drops were regularly pictured to detect the crystallization events and study the effect of the lanthanide additive. A typical comparison is reported in Figure 2; the protein alone
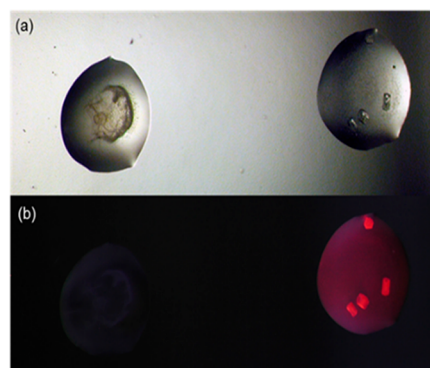

Figure 2. Crystallization drops of Ec-AcrB alone (left) and in the presence of $[Eu(DPA)_3]^{3-}$ (right) in transmission (a) or under 315 nm irradiation (b).

precipitates as an amorphous slurry, whereas in the presence of $[Eu(DPA)_3]^{3-}$, exploitable crystals have been obtained that were strongly luminescent under UV irradiation (Figure 2). However, after analysis, these crystals did not contain any protein and are simply composed of pure $[Eu(DPA)_3]^{3-}$. Consequently, self-crystallization of such a lanthanide complex is a typical example of false positive hampering practical cocrystallization experiments with proteins.

Another surprising result was obtained during the systematic study of the protein fractions from the marine organism *M. thermolithotrophicus* in the presence of TbXo4. This research project allows us to solve four unknown protein structures,[23,30,31] including AdkA (66.12 kDa). The structure of AdkA (PDB 6HF7) was solved at 1.96 Å resolution in a condition containing 50 mM magnesium ion [see the Supporting Information (SI) for details]. The asymmetric unit contains the biological unit consisting in a homotrimer (Figure 3a) and four bound Tb-Xo4, among which two, with the highest occupancy (0.7), were unambiguously modeled. The latter are located at the same location on two AdkA monomers and thus involve an identical supramolecular interaction network. The analogous site on the third protein
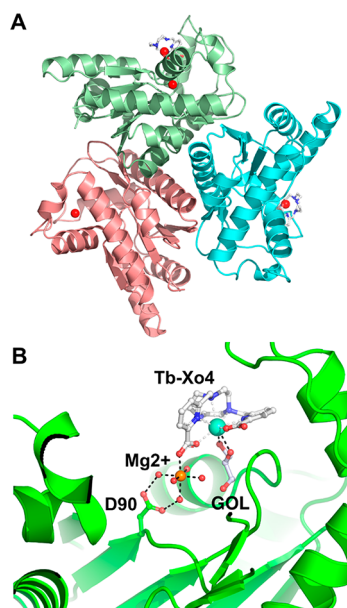
Figure 3. (A) Trimer of AdkA cocrystallized with 10 mM Tb-Xo4 (Tb^{3+} in blue) in the presence of MgCl$_2$ (Mg^{2+} in gray). (B) Insights into the Tb-Xo4 main binding site (GOL = glycerol).

monomer is unoccupied. A detailed investigation of the binding pocket reveals the involvement of a hydrated magnesium bridging the crystallophore to the surface protein through aspartate 90 (Figure 3b). The second feature is the presence of a glycerol molecule contained in the protein buffer, completing the coordination sphere of the terbium ion. Starting from this crystal structure, this main binding site was investigated using density functional theory calculation (see the SI for details). The strongest interaction involves the hydrated magnesium and the aspartate residue (D90) ensuring the binding of the crystallophore to the AdkA surface and corresponding to an interaction energy of −25.3 kcal·mol^{-1} (Figure S1 and Table S1). This surprising formation of a {Tb-Xo4/Mg^{2+}} adduct in the interaction pocket of AdkA can be compared to the recently reported structure of the protein FprA with the observation of a {FprA/Tb-Xo4/Ca^{2+}} adduct.[32] In both cases, the alkaline-earth cation (Mg^{2+} or Ca^{2+}) was present in the crystallization mixture as well as a glycerol molecule, near Tb-Xo4.

These unexpected and reproducible results prompted us to investigate the behavior of the two complexes Na$_3$[Eu(DPA)$_3$] and Tb-Xo4 with different constituents of several commercial crystallization kits routinely used for automated crystallization experiments at the HTXlab (EMBL, Grenoble, France). These kits encompassed a total of 576 conditions depending on the pH and nature of the buffer (TRIS, MES, HEPES, citric acid, sodium acetate, etc.), the presence of salts at different concentrations [NaCl, (NH$_4$)$_2$SO$_4$, MgCl$_2$, CaCl$_2$, etc.], or the organic molecules [such as poly(ethylene glycol), methyl-2,4-pentanediol, isopropyl alcohol, etc.]. In order to evaluate the propensity of both lanthanide additives to generate reproducible false positives in crystallization media, the behavior of the lanthanide complexes was tested in each condition in the absence of any protein. Indeed, from our experience, the addition of different macromolecules induces slight variations in the outcomes of such an experiment and impedes any general observation.

The experiment was performed by mixing an equal volume of the additive solution at the desired concentration (10−100 mM for Tb-Xo4 and 25−100 mM for Na$_3$[Eu(DPA)$_3$]) with the crystallization solution to form the sitting drop (Tables S2 and S3). Drops were then evaluated for the presence of potential self-crystallization or precipitate formation by conventional imaging techniques and for the instability of the complexes by the disappearance of the lanthanide emission signal under UV irradiation.

Interestingly, spontaneous crystallization of Na$_3$[Eu(DPA)$_3$] was observed in 10% of the conditions at 25 mM, and this ratio increased up to 30% at 100 mM. Analysis of these conditions indicated that high concentrations of salt [such as NaCl, (NH$_4$)$_2$SO$_4$, etc.], typically higher than 0.8 M, and the presence of divalent salts (Ca^{2+}, Mg^{2+}) and 2-methyl-2,4-pentanediol or isopropyl alcohol favored self-crystallization of the tris(dipicolinate) complex. If the increase of the anionic strength and the decrease of the solubility of the complex in the presence of alcohol in the media are classical ways to promote crystallization, the effect of divalent cations was less expected. Therefore, the reactions of Na$_3$[Eu(DPA)$_3$] with alkaline-earth salts (CaCl$_2$, MgCl$_2$, and BaCl$_2$) were undertaken independently. Slow diffusion of the divalent alkaline-earth chloride solutions into an aqueous Na$_3$[Eu(DPA)$_3$] solution results in the fast formation of transparent crystals, almost insoluble in water and organic solvents. Diffraction experiments performed on these crystals revealed the formation of structures of the respective formulas (Mg-(H$_2$O)$_6$)$_3$[Eu(DPA)$_3$]$_2$·7H$_2$O (**1**) and {(Ca(H$_2$O)$_4$)$_3$[Eu-(DPA)$_3$]$_2$}$_n$·10nH$_2$O (**2**) and of the previously reported {[Eu(DPA)$_3$]$_2$Ba$_3$(H$_2$O)$_{16}$]·4H$_2$O}$_n$.[33−35] Crystal data and refinement parameters are given in Table S4, whereas selected bond lengths are compiled in Tables S5 and S7. In all cases, the Na$^+$ counterion was completely replaced by Ca^{2+}/Mg^{2+}/Ba^{2+}, respectively, which are themselves coordinated by water or by [Eu(DPA)$_3$]$^{3-}$ carboxylate, forming 3-to-2 assemblies with the complex (Figures 4 and 5) and explaining the strong decrease of the solubility. While the structure of **1** exhibits isolated [Eu(DPA)$_3$]$^{3-}$ and [Mg(H$_2$O)$_6$]$^{2+}$ units (Figure 4), **2** presents
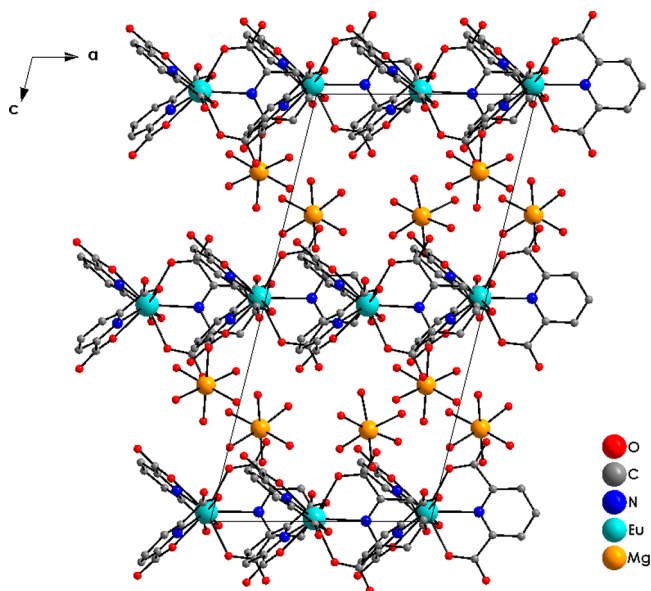

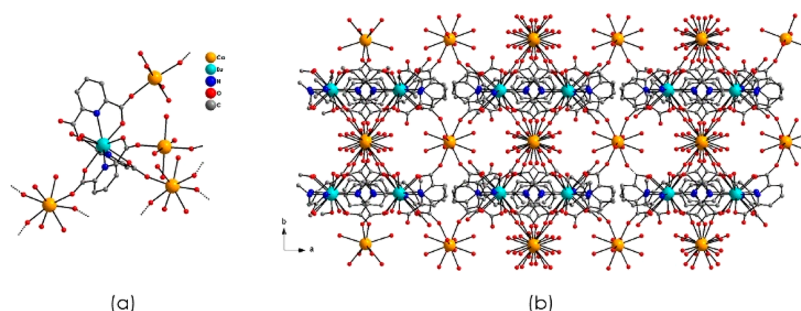**Figure 4.** Projection along the b axis of the crystal packing of **1**.

Figure 5. (a) Molecular building block of complex **2**. (b) Projection along the c axis of the unit cell in order to highlight the $[Ca(H_2O)_n]^{2+}$ (in orange) and $[Eu(DPA)_3]^{3-}$ (in blue) planes running perpendicularly to the b axis of the unit cell. For clarity, hydrogen atoms and noncoordinated water molecules have been removed.

a 3D network with $[Eu(DPA)_3]^{3-}$ building blocks connected together through $[Ca(H_2O)_2]^{2+}$ or $[Ca(H_2O)_4]^{2+}$ bridges (Figure 5). In the latter case, a second oxygen atom of one (for two ligands) or both (for one ligand) of the two DPA acid functions completes the Ca^{2+} environment and then creates links in the three directions between europium(III) and calcium(II) complexes. The geometric configurations of both complexes were analyzed with the help of the *SHAPE2.1* program (Tables S6 and S8). The investigation of the precise configurations demonstrated that each Eu^{3+} cation environment within the **1** and **2** structures fits well with the nonacoordinate capped square antiprism (CSAPR-9, C_{4v}) and tricapped trigonal prism (TCTPR-9, D_{3h}), respectively. All of the Eu−O and Eu−N bond lengths are in good agreement with those observed in the literature.[36−39]

During automated crystallization experiments, we noticed that the characteristic red emission of $[Eu(DPA)_3]^{3-}$ disappeared systematically for all of the formulations containing transition-metal ions (with M^{2+} = Cd^{2+}, Zn^{2+}, Ni^{2+}, Fe^{2+}, Co^{2+}, and a mixture). Measurements of the $Na_3[Eu(DPA)_3]$ emissions were performed in the presence of MCl_2 in a diluted water solution (lanthanide concentration at 1 mM; Figure S5). Interestingly, the luminescence of $[Eu(DPA)_3]^{3-}$ was rapidly quenched after the addition of 1 equiv of MCl_2, and about 80% of the emission had disappeared. This competition experiment has also been performed at a concentration closer to the crystallization conditions: slow diffusion of a $CuCl_2$ solution (50 mM) in $Na_3[Eu(DPA)_3]$ (50 mM) led to the formation of crystals of $\{Cu(DPA)(H_2O)_2\}_n$ (**3**) suitable for X-ray diffraction analysis (Figure 6 and Tables S3 and S8).[40] Copper(II) is coordinated to one deprotonated ligand (two oxygen and one nitrogen

atoms) and two water molecules. The distorted cation octahedral ML_6 $\{O_5N_1\}$ environment is then completed by one oxygen atom (O3) belonging to one neighboring complex unit. This bridge leads to the formation of chains of complexes running along the c axis of the unit cell with a $Cu^{2+}\cdots Cu^{2+}$ intrachain distance equal to 3.87 Å. All of the Cu−N and Cu−O bond lengths and O−Cu−O and N−Cu−O bond angles are in agreement with those usually listed in the literature for the corresponding systems.[41] $\{Cu(DPA)(H_2O)_2\}_n$ chains perfectly stack one above the other in the a direction of the unit cell and slightly shift in the c direction of the unit cell. Structural cohesion between chains is assumed by weak interactions (hydrogen bonds and van der Waals interactions). These results indicated that a transmetalation reaction occurs very rapidly between $[Eu(DPA)_3]^{3-}$ and transition-metal cations, leading to destruction of the lanthanide complex in solution.

These few selected examples are specific to the respective impacts of alkaline earths and transition metals. The trianionic $[Eu(DPA)_3]^{3-}$ suffers from a high affinity to divalent cations and the lability of dipicolinate ligands, which allow possible transmetalation reactions; both mechanisms tend to form lower solubility products. It is also worth noticing that both the complex and its products keep high symmetry (D_3 and C_{2v}), which will enable easier packing as crystalline precipitates. All of these drawbacks prompted us to design the crystallophore based on a macrocyclic ligand to improve the stability and exhibited a cationic charge to limit the interaction with dications.

As expected, the behavior of the Tb-Xo4 complex is completely different. The automated crystallization experiments revealed that all drops remained perfectly clear at 10 mM concentration. At 100 mM, only three conditions over 576 led to the formation of microcrystalline precipitates (Figures S2−S4). These conditions contain, among others, ammonium fluoride, calcium acetate, or ammonium sulfate in the presence of poly(ethylene glycol). The obtained microcrystals did not present optimal quality for X-ray diffraction, and we have been unable to reproduce them in larger batches for the preparation of well-diffracting crystals. TbXo4 crystals of the global formula $[Tb_4L_4(H_2O)_4]Cl_4\cdot 15H_2O$ (**4**) were hardly obtained from the slow evaporation of a water/acetonitrile mixture (Tables S3, S9, and S10). These crystals are luminescent in the green region upon UV irradiation (Figure 7).

In the structure, one terbium(III) atom is coordinated in a $\{N_5O_4\}$ environment. The deprotonated ligand L^{2-} is coordinated by two oxygen atoms from the carboxylate moieties and five nitrogen atoms from the pyridine and
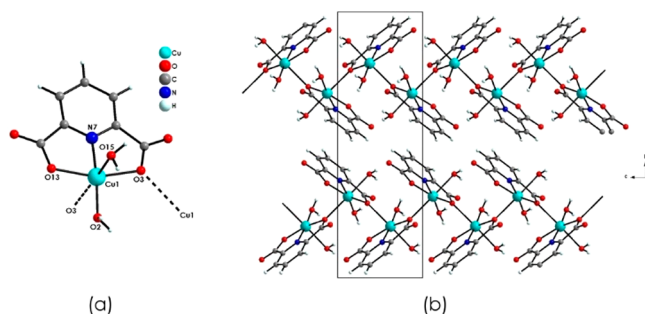

Figure 6. (a) Molecular unit of **3** with important labels. (b) Projection along the a axis of the unit cell of $\{Cu(DPA)(H_2O)_2\}_n$ chains running along the c axis of the unit cell.
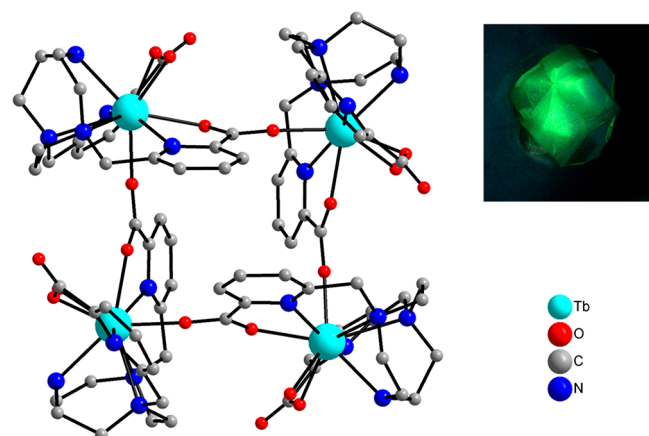
Figure 7. Structure of complex **4**. For clarity, hydrogen atoms and noncoordinated chloride and water molecules have been removed. Inset: Picture of one crystal of complex **4** under UV irradiation (λ_{ex} = 254 nm).

triazacyclononane macrocycle. The Tb−O bond lengths (2.403 Å) are shorter than the Tb−N ones (2.566 Å) and are in good agreement with those previously reported in the literature for identical complexes.[42] The coordination sphere is completed by the two oxygen atoms from one water molecule with a Tb−O bond length (2.449 Å) comparable to those of the other Tb−O(L) and one oxygen atom from the carbonyl fragment belonging to the ligand of a neighboring complex with a short Tb−O bond (2.265 Å). Thus, four complexes assemble in a remarkable tetrameric supramolecular architecture (Figure 7). The charge balance is ensured by the presence of four Cl⁻ anions within the unit cell. A total of 15 noncoordinated water molecules also cocrystallize within the unit cell. Both of these noncoordinated molecules or anions are located in channels running along the *c* axis of the unit cell and generated by the global complex packing.

In addition, the stability experiments in solution were performed with Tb-Xo4, in the same conditions as those with Na₃[Eu(DPA)₃]. First, the addition of 1 equiv of MCl₂ to a Tb-Xo4 solution led to a much slower decrease of the green luminescence observed over several days (Figure S6) compared to the almost instantaneous luminescence decrease observed in Na₃[Eu(DPA)₃] (Figure S4). Second, in the presence of alkaline-earth salts (MgCl₂, CaCl₂, and BaAc₂; 1−10 equiv), no variation of the luminescence intensity of Tb-Xo4 was observed for days (Figure S7). All results indicated that a transmetalation reaction occurs between the two lanthanide complexes and transition-metal cations but with a very different kinetic underlining a higher stability for the macrocyclic Tb-Xo4 complex compared to the homoleptic [Eu(DPA)₃]³⁻ featuring three tridentate ligands. In addition, in the presence of alkaline-earth salts, Tb-Xo4 is highly stable, whereas [Eu(DPA)₃]³⁻ precipitates and/or self-crystallizes.

◼ CONCLUSION

In conclusion, we started undertaking the systematic analysis of the influence of the commercial crystallization kit composition on the efficiency of two lanthanide-based additives: Na₃[Eu-(DPA)₃] and Tb-Xo4. The tris(dipicolinate) complex presents a lower chemical stability and a strong tendency toward self-crystallization detrimental for its use in a high-throughput robotized crystallization platform. On the other hand, Tb-Xo4,

based on a macrocyclic ligand, is perfectly soluble in the crystallization media, is stable in the presence of alkaline-earth dications, and slowly decomposed (within days) by transmetalation with transition metals. This article also outlines the interest of interactions between the crystallization mixture component and Tb-Xo4, leading to the formation of more complex adducts like {AdkA/Tb-Xo4/Mg²⁺/glycerol} or {FprA/Tb-Xo4/Ca²⁺/glycerol} in the protein binding sites. The observation of such multicomponent adducts illustrated the complexity and versatility of the supramolecular chemistry occurring at the surface of proteins. The role of such adducts during the crystallization process is currently under investigation.

◼ ASSOCIATED CONTENT

◼ AUTHOR INFORMATION

Corresponding Authors

Olivier Maury − *Laboratoire de Chimie, ENS de Lyon, CNRS, UMR 5182, Université Lyon, Lyon F-69342, France;* ⓞ orcid.org/0000-0002-4639-643X; Email: olivier.maury@ens-lyon.fr

François Riobé − *Laboratoire de Chimie, ENS de Lyon, CNRS, UMR 5182, Université Lyon, Lyon F-69342, France;* ⓞ orcid.org/0000-0001-6746-8132; Email: francois.riobe@ens-lyon.fr

Eric Girard − *CEA, CNRS, IBS, Université Grenoble Alpes, Grenoble F-38000, France;* ⓞ orcid.org/0000-0002-5758-6095; Email: eric.girard@ibs.fr

Authors

Amandine Roux − *Laboratoire de Chimie, ENS de Lyon, CNRS, UMR 5182, Université Lyon, Lyon F-69342, France; Polyvalan, Lyon F-69342, France*

Romain Talon − *CEA, CNRS, IBS, Université Grenoble Alpes, Grenoble F-38000, France*

Zaynab Alsalman − *CEA, CNRS, IBS, Université Grenoble Alpes, Grenoble F-38000, France*

Sylvain Engilberge − *CEA, CNRS, IBS, Université Grenoble Alpes, Grenoble F-38000, France*

Anthony D'Aléo − *Laboratoire de Chimie, ENS de Lyon, CNRS, UMR 5182, Université Lyon, Lyon F-69342, France*

Sebastiano Di Pietro − *Laboratoire de Chimie, ENS de Lyon, CNRS, UMR 5182, Université Lyon, Lyon F-69342, France*

Adeline Robin − *CEA, CNRS, IBS, Université Grenoble Alpes, Grenoble F-38000, France*

Alessio Bartocci − *Laboratoire de Chimie, ENS de Lyon, CNRS, UMR 5182, Université Lyon, Lyon F-69342, France*

Guillaume Pilet − *CNRS UMR 5615, Université Lyon, Villeurbanne Cedex F-69622, France*

Elise Dumont − *Laboratoire de Chimie, ENS de Lyon, CNRS, UMR 5182, Université Lyon, Lyon F-69342, France; Institut Universitaire de France, Paris 75005, France;* ⊙ orcid.org/0000-0002-2359-111X

Tristan Wagner − *Microbial Protein Structure Group, Max Planck Institute for Terrestrial Microbiology, Marburg D-35043, Germany; Microbial Metabolism Group, Max Planck Institute for Marine Microbiology, Bremen 35043, Germany*

Seigo Shima − *Microbial Protein Structure Group, Max Planck Institute for Terrestrial Microbiology, Marburg D-35043, Germany*

Complete contact information is available at:
https://pubs.acs.org/10.1021/acs.inorgchem.1c01635

Notes
The authors declare no competing financial interest.

■ REFERENCES

(1) Terwilliger, T. C.; Stuart, D.; Yokoyama, S. Lessons from Structural Genomics. *Annu. Rev. Biophys.* **2009**, *38* (1), 371−383.

(2) Khurshid, S.; Saridakis, E.; Govada, L.; Chayen, N. E. Porous nucleating agents for protein crystallization. *Nat. Protoc.* **2014**, *9* (7), 1621−1633.

(3) McPherson, A.; Gavira, J. Introduction to protein crystallization. *Acta Crystallogr., Sect. F: Struct. Biol. Commun.* **2014**, *70*, 2−20.

(4) Santarsiero, B. D.; Yegian, D. T.; Lee, C. C.; Spraggon, G.; Gu, J.; Scheibe, D.; Uber, D. C.; Cornell, E. W.; Nordmeyer, R. A.; Kolbe, W. F.; Jin, J.; Jones, A. L.; Jaklevic, J. M.; Schultz, P. G.; Stevens, R. C. An approach to rapid protein crystallization using nanodroplets. *J. Appl. Crystallogr.* **2002**, *35*, 278−281.

(5) Brown, J.; Walter, T. S.; Carter, L.; Abrescia, N. G. A.; Aricescu, A. R.; Batuwangala, T. D.; Bird, L. E.; Brown, N.; Chamberlain, P. P.; Davis, S. J.; Dubinina, E.; Endicott, J.; Fennelly, J. A.; Gilbert, R. J. C.; Harkiolaki, M.; Hon, W. C.; Kimberley, F.; Love, C. A.; Mancini, E. J.; Manso-Sancho, R.; Nichols, C. E.; Robinson, R. A.; Sutton, G. C.; Schueller, N.; Sleeman, M. C.; Stewart-Jones, G. B.; Vuong, M.; Welburn, J.; Zhang, Z.; Stammers, D. K.; Owens, R. J.; Jones, E. Y.; Harlos, K.; Stuart, D. I. A procedure for setting up high-throughput nanolitre crystallization experiments. II. Crystallization results. *J. Appl. Crystallogr.* **2003**, *36*, 315−318.

(6) Hendrickson, W. A. Anomalous diffraction in crystallographic phase evaluation. *Q. Rev. Biophys.* **2014**, *47* (1), 49−93.

(7) Doublié, S. Preparation of selenomethionyl proteins for phase determination. *Methods in Enzymology*; Academic Press, 1997; Vol. 276, pp 523−530.

(8) D'Arcy, A.; Mac Sweeney, A.; Haber, A. Using natural seeding material to generate nucleation in protein crystallization experiments. *Acta Crystallogr., Sect. D: Biol. Crystallogr.* **2003**, *59*, 1343−1346.

(9) Georgieva, D. G.; Kuil, M. E.; Oosterkamp, T. H.; Zandbergen, H. W.; Abrahams, J. P. Heterogeneous nucleation of three-dimensional protein nanocrystals. *Acta Crystallogr., Sect. D: Biol. Crystallogr.* **2007**, *63*, 564−570.

(10) Saridakis, E.; Khurshid, S.; Govada, L.; Phan, Q.; Hawkins, D.; Crichlow, G. V.; Lolis, E.; Reddy, S. M.; Chayen, N. E. Protein crystallization facilitated by molecularly imprinted polymers. *Proc. Natl. Acad. Sci. U. S. A.* **2011**, *108* (27), 11081.

(11) Khurshid, S.; Govada, L.; El-Sharif, H. F.; Reddy, S. M.; Chayen, N. E. Automating the application of smart materials for protein crystallization. *Acta Crystallogr., Sect. D: Biol. Crystallogr.* **2015**, *71*, 534−540.

(12) Bijelic, A.; Rompel, A. The use of polyoxometalates in protein crystallography - An attempt to widen a well-known bottleneck. *Coord. Chem. Rev.* **2015**, *299*, 22−38.

(13) Breibeck, J.; Bijelic, A.; Rompel, A. Transition metal-substituted Keggin polyoxotungstates enabling covalent attachment to proteinase K upon co-crystallization. *Chem. Commun.* **2019**, *55* (77), 11519−11522.

(14) Mac Sweeney, A.; Chambovey, A.; Wicki, M.; Muller, M.; Artico, N.; Lange, R.; Bijelic, A.; Breibeck, J.; Rompel, A. The crystallization additive hexatungstotellurate promotes the crystallization of the HSP70 nucleotide binding domain into two different crystal forms. *PLoS One* **2018**, *13* (6), e0199639.

(15) Bijelic, A.; Rompel, A. Polyoxometalates: more than a phasing tool in protein crystallography. *ChemTexts* **2018**, *4* (3), 10.

(16) McGovern, R. E.; Fernandes, H.; Khan, A. R.; Power, N. P.; Crowley, P. B. Protein camouflage in cytochrome c-calixarene complexes. *Nat. Chem.* **2012**, *4* (7), 527−33.

(17) McGovern, R. E.; Feifel, S. C.; Lisdat, F.; Crowley, P. B. Microscale Crystals of Cytochrome c and Calixarene on Electrodes: Interprotein Electron Transfer between Defined Sites. *Angew. Chem., Int. Ed.* **2015**, *54* (21), 6356−6359.

(18) Guagnini, F.; Antonik, P. M.; Rennie, M. L.; O'Byrne, P.; Khan, A. R.; Pinalli, R.; Dalcanale, E.; Crowley, P. B. Cucurbit[7]uril-Dimethyllysine Recognition in a Model Protein. *Angew. Chem., Int. Ed.* **2018**, *57* (24), 7126−7130.

(19) Engilberge, S.; Rennie, M. L.; Dumont, E.; Crowley, P. B. Tuning Protein Frameworks via Auxiliary Supramolecular Interactions. *ACS Nano* **2019**, *13* (9), 10343−10350.

(20) Pompidor, G.; D'Aleo, A.; Vicat, J.; Toupet, L.; Giraud, N.; Kahn, R.; Maury, O. Protein crystallography through supramolecular interactions between a lanthanide complex and arginine. *Angew. Chem., Int. Ed.* **2008**, *47* (18), 3388−3391.

(21) Engilberge, S.; Riobe, F.; Di Pietro, S.; Lassalle, L.; Coquelle, N.; Arnaud, C. A.; Pitrat, D.; Mulatier, J. C.; Madern, D.; Breyton, C.; Maury, O.; Girard, E. Crystallophore: a versatile lanthanide complex for protein crystallography combining nucleating effects, phasing properties, and luminescence. *Chem. Sci.* **2017**, *8* (9), 5909−5917.

(22) Ramberg, K. O.; Engilberge, S.; Skorek, T.; Crowley, P. B. Facile Fabrication of Protein−Macrocycle Frameworks. *J. Am. Chem. Soc.* **2021**, *143* (4), 1896−1907.

(23) Engilberge, S.; Wagner, T.; Santoni, G.; Breyton, C.; Shima, S.; Franzetti, B.; Riobe, F.; Maury, O.; Girard, E. Protein crystal structure determination with the crystallophore, a nucleating and phasing agent. *J. Appl. Crystallogr.* **2019**, *52* (4), 722−731.

(24) de Wijn, R.; Hennig, O.; Roche, J.; Engilberge, S.; Rollet, K.; Fernandez-Millan, P.; Brillet, K.; Betat, H.; Morl, M.; Roussel, A.; Girard, E.; Mueller-Dieckmann, C.; Fox, G. C.; Olieric, V.; Gavira, J. A.; Lorber, B.; Sauter, C. A simple and versatile microfluidic device for efficient biomacromolecule crystallization and structural analysis by serial crystallography. *IUCrJ* **2019**, *6* (3), 454−464.

(25) Rempel, S.; Colucci, E.; de Gier, J. W.; Guskov, A.; Slotboom, D. J. Cysteine-mediated decyanation of vitamin B12 by the predicted membrane transporter BtuM. *Nat. Commun.* **2018**, *9* (1), 3038.

(26) Hajj Chehade, M.; Pelosi, L.; Fyfe, C. D.; Loiseau, L.; Rascalou, B.; Brugière, S.; Kazemzadeh, K.; Vo, C.-D.-T.; Ciccone, L.; Aussel, L.; Couté, Y.; Fontecave, M.; Barras, F.; Lombard, M.; Pierrel, F. A Soluble Metabolon Synthesizes the Isoprenoid Lipid Ubiquinone. *Cell Chem. Biol.* **2019**, *26* (4), 482−492.

(27) Roche, J.; Girard, E.; Mas, C.; Madern, D. The archaeal LDH-like malate dehydrogenase from Ignicoccus islandicus displays dual substrate recognition, hidden allostery and a non-canonical tetrameric oligomeric organization. *J. Struct. Biol.* **2019**, *208* (1), 7−17.

(28) Schada von Borzyskowski, L.; Severi, F.; Krüger, K.; Hermann, L.; Gilardet, A.; Sippel, F.; Pommerenke, B.; Claus, P.; Cortina, N. S.; Glatter, T.; Zauner, S.; Zarzycki, J.; Fuchs, B. M.; Bremer, E.; Maier, U. G.; Amann, R. I.; Erb, T. J. Marine Proteobacteria metabolize glycolate via the β-hydroxyaspartate cycle. *Nature* **2019**, *575* (7783), 500−504.

(29) Belot, L.; Ouldali, M.; Roche, S.; Legrand, P.; Gaudin, Y.; Albertini, A. A. Crystal structure of Mokola virus glycoprotein in its post-fusion conformation. *PLoS Pathog.* **2020**, *16* (3), e1008383.

(30) Bernhardsgrütter, I.; Vögeli, B.; Wagner, T.; Peter, D. M.; Cortina, N. S.; Kahnt, J.; Bange, G.; Engilberge, S.; Girard, E.; Riobé, F.; Maury, O.; Shima, S.; Zarzycki, J.; Erb, T. J. The multicatalytic compartment of propionyl-CoA synthase sequesters a toxic metabolite. *Nat. Chem. Biol.* **2018**, *14* (12), 1127−1132.

(31) Vogeli, B.; Engilberge, S.; Girard, E.; Riobe, F.; Maury, O.; Erb, T. J.; Shima, S.; Wagner, T. Archaeal acetoacetyl-CoA thiolase/HMG-CoA synthase complex channels the intermediate via a fused CoA-binding site. *Proc. Natl. Acad. Sci. U. S. A.* **2018**, *115* (13), 3380−3385.

(32) Engilberge, S.; Riobe, F.; Wagner, T.; Di Pietro, S.; Breyton, C.; Franzetti, B.; Shima, S.; Girard, E.; Dumont, E.; Maury, O. Unveiling the Binding Modes of the Crystallophore, a Terbium-based Nucleating and Phasing Molecular Agent for Protein Crystallography. *Chem. - Eur. J.* **2018**, *24* (39), 9739−9746.

(33) Zhao, X.-Q.; Zuo, Y.; Gao, D.-L.; Zhao, B.; Shi, W.; Cheng, P. Syntheses, Structures, and Luminescence Properties of a Series of Ln(III)−Ba(II) Heterometal-Organic Frameworks. *Cryst. Growth Des.* **2009**, *9* (9), 3948−3957.

(34) Chen, Y.; Li, L.; Zhang, Q.; Liu, S.; Tian, Z.; Ju, Z. Effects of calcium ions on crystal structure and luminescence properties of six rare earth metal complexes. *J. Solid State Chem.* **2020**, *281*, 121053.

(35) Chen, Y.; Zhao, X.; Gao, R.; Ruan, Z.; Lin, J.; Liu, S.; Tian, Z.; Chen, X. Temperature-induced solvent assisted single-crystal-to-single-crystal transformation of Mg(II)-Ln(III) heterometallic coordination polymers. *J. Solid State Chem.* **2020**, *292*, 121674.

(36) Tancrez, N.; Feuvrie, C.; Ledoux, I.; Zyss, J.; Toupet, L.; Le Bozec, H.; Maury, O. Lanthanide Complexes for Second Order Nonlinear Optics: Evidence for the Direct Contribution of f Electrons to the Quadratic Hyperpolarizability. *J. Am. Chem. Soc.* **2005**, *127* (39), 13474−13475.

(37) D'Aleo, A.; Pompidor, G.; Elena, B.; Vicat, J.; Baldeck, P. L.; Toupet, L.; Kahn, R.; Andraud, C.; Maury, O. Two-photon microscopy and spectroscopy of lanthanide bioprobes. *ChemPhysChem* **2007**, *8* (14), 2125−2132.

(38) D'Aléo, A.; Toupet, L.; Rigaut, S.; Andraud, C.; Maury, O. Guanidinium as powerful cation for the design of lanthanate tris-dipicolinate crystalline materials: Synthesis, structure and photophysical properties. *Opt. Mater.* **2008**, *30* (11), 1682−1688.

(39) Mooibroek, T. J.; Gamez, P.; Pevec, A.; Kasunic, M.; Kozlevcar, B.; Fu, W. T.; Reedijk, J. Efficient, stable, tunable, and easy to synthesize, handle and recycle luminescent materials: [H_2NMe_2]$_3$[Ln(III)(2,6-dipicolinolate)$_3$] (Ln = Eu, Tb, or its solid solutions). *Dalton Trans* **2010**, *39* (28), 6483−6487.

(40) The structure of this complex was previously reported in: Xie, C.; Zhang, Z.; Wang, X.; Liu, X.; Shen, G.; Wang, R.; Shen, D. The Synthesis and Structure of a Novel 1D copper(II) Weak Coordination Polymer with 2,6-Pyridinedicarboxylic Acid. *J. Coord. Chem.* **2004**, *57*, 1173−1178.

(41) Sileo, E. E.; Rigotti, G.; Rivero, B. E.; Blesa, M. A. Kinetic study of the thermal dehydration of copper(II) dipicolinates: Crystal and molecular structure of Cu(II) (Pyridine 2,6-Dicarboxylato) DI- and Trihydrated. *J. Phys. Chem. Solids* **1997**, *58* (7), 1127−1135.

(42) Nocton, G.; Nonat, A.; Gateau, C.; Mazzanti, M. Water Stability and Luminescence of Lanthanide Complexes of Tripodal Ligands Derived from 1,4,7-Triazacyclononane: Pyridinecarboxamide versus Pyridinecarboxylate Donors. *Helv. Chim. Acta* **2009**, *92* (11), 2257−2273.